International Journal of Mechanical Engineering and Robotics Research

ISSN 2278 – 0149 www.ijmerr.com
Vol. 3, No. 3, July 2014

Research Paper

CIMEV: CASTER-WHEELED INDEPENDENT-MOTOR-DRIVEN ELECTRIC VEHICLE, ITS DESIGN AND CONTROL AS A FUTURE MOBILITY SOLUTION

Yunha Kim[1]*, Kanghyun Nam[1], Hiroshi Fujimoto[1] and Yoichi Hori[1]

*Corresponding Author: Yunha Kim, ✉ yunha.kim@hori.k.u-tokyo.ac.jp

This paper presents a novel chassis structure for advanced mobility platforms, using caster wheels with disturbance observers, and independent driving motors. The system consists of two independent driving wheels and two caster wheels. The proposed configuration enables the vehicle to have: a low mechanical stiffness against the direct yaw moment input because caster wheels are free to rotate; and high static stability because of the four wheels having a large base geometry. In addition, by introducing disturbance observers, the vehicle was given enhanced mobility and safety characteristics. A number of advantages, which include small-radius turning, under-steer gradient control, load transfer estimation, of the proposed system are shown and discussed with experimental results throughout the paper.

Keywords: Mobility platform, Mobile robot, Caster wheel, Disturbance observer, Motion control

INTRODUCTION

Utilizing the advantages of electric motor described below (Hori, 2004), many motion control strategies for Electric Vehicles (EVs) such as anti-slip traction control, running stability control, and range extension control, have been introduced in recent years (Ando *et al.*, 2009; Nam *et al.*, 2012; and Sumiya *et al.*, 2012). These control methods turned out to be effective hence EVs can run more safely and energy-efficiently than conventional Internal Combustion Engine Vehicles (ICEVs).

- Torque generation of an electric motor is very quick and accurate.
- A motor can be attached to each wheel.
- Motor torque can be measured easily.

In addition to aforementioned properties, vehicle electrification enables EVs to excel ICEVs in terms of two-dimensional vehicle

[1] Department of Electrical Engineering, The University of Tokyo, 3-7-1 Hongo, Bunkyo-ku, Tokyo, Japan.

motion, by assigning two inputs—the steering and the direct yaw moment—while the conventional vehicles have only the steering input. The torque vectoring technology for ICEVs (Mohan, 2005; and Sawase *et al.*, 2006) seems to be similar to the direct yaw moment input, however it is obvious that the controllability and the system response of EVs are much better than those of ICEVs due to the reasons listed above.

However, most of these research works are based on the four-wheeled vehicle chassis structure with the conventional mechanical steering system, which has not changed from the beginning of the mass production of the Ford Model T in 1908. It was originally designed and has been optimized for an internal combustion engine to transmit power to each of the driving wheels. Consequently it is clear that to use the conventional chassis structure for the independent motor driven EVs is a waste of ability, hence motivates this work.

Despite the underlying importance, it seems that there have been only a few attempts to provide a new chassis structure for the independent motor driven EVs. In 1968, Slay (Slay, 1968) invented an electric-motor-driven vehicle that could change direction at right angles using powered caster wheels. Similarly, Lam et al. designed a novel type all wheel driven and steered EV (Lam *et al.*, 2010). These systems imply a number of possibilities of what electric vehicles can bring about. Yet such systems are still too expensive in terms of the number of actuators and control efforts. Slay's system needs analyses on stability and maneuverability. Lam's work is rather focused on the driver interface, thus the vehicle dynamics itself has to be investigated more in various speed ranges. Another design proposed by Ebihara *et al.* (2011) gives some hints for the new design of micro EVs. It uses only the moment steering showing that the performance is good enough to deal with given tasks. The free rotating casters work well on the irregular terrain—a grass field. However, it still needs improvements, if postulating personal mobility applications, in high speed running performance considering the lateral forces when cornering.

Besides EVs, some attempts to provide high agility for mobility platforms can also be found. Swisher's invention of 1952 (Swisher *et al.*, 1952) contributed to the mobility of lawn mowers which require quickness in their motion due to the fact that their operation space is usually restricted, and has obstacles and ditches.

Brienza's work on a novel steering linkage (Brienza *et al.*, 1999), and Borenstein's mobile robot platform (Borenstein *et al.*, 1985) are highly applicable and useful to the vehicles in the field of welfare and social security.

All three of them, however, operate in a relatively low speed range where controllability and stability problems of vehicle dynamics can be neglected, hence they are not taken into account. As for future personal mobility solutions, the dynamics of the vehicle in the high speed range such as steering and cornering characteristics becomes important, because it is deeply related to the safety issues. The authors present considerations on these issues, which makes a part of contributions of this work.

In this work, a novel chassis structure using caster wheels and independent driving motors is proposed. Provided with four wheels, the system is designed to be structurally stable, and with caster wheels on the front axle the proposed system is able to fully utilize the two inputs—the steering angle and the direct yaw moment—in two-dimensional vehicle motion. The design philosophy and the control strategies are developed and discussed in the following sections throughout the paper.

STUDY ON WHEEL PLACEMENTS

To seek the most appropriate chassis structure for an independent-motor-driven EV, it is necessary to discuss the wheel placements and their effects on the vehicle behavior first.

In this section, some general wheel placements and corresponding dynamics are introduced. Then the relevant stability evaluation criteria are shown, and followed by discussion on the compatibility with the EV motion control.

Wheel Placements and Dynamics

Three generally thinkable kinds of vehicle wheel placements and their dynamics are introduced here: three-wheeled vehicle model with one wheel front; three-wheeled vehicle model with one wheel rear; and four-wheeled vehicle model. It is assumed that each of the dynamic models has two independent driving motors in the system for fair comparison. The effect of the suspension system is neglected for simplicity, assuming that the vehicle would mainly run on the paved roads where the tire-ground contact is secured to a certain degree.

Major assumptions for the system analyses are: all vehicle models introduced here share the vehicle parameters shown in Nomenclature, which are equivalent to those of the experimental vehicle CIMEV (Figure 1); each system has two independent driving motors within, and the steering wheels are on the front axle; the effect of the suspension

Figure 1: Three Vehicle Models Used in the Analyses. Frame of Reference, Center of Gravity, Motor Position, and etc., are Indicated

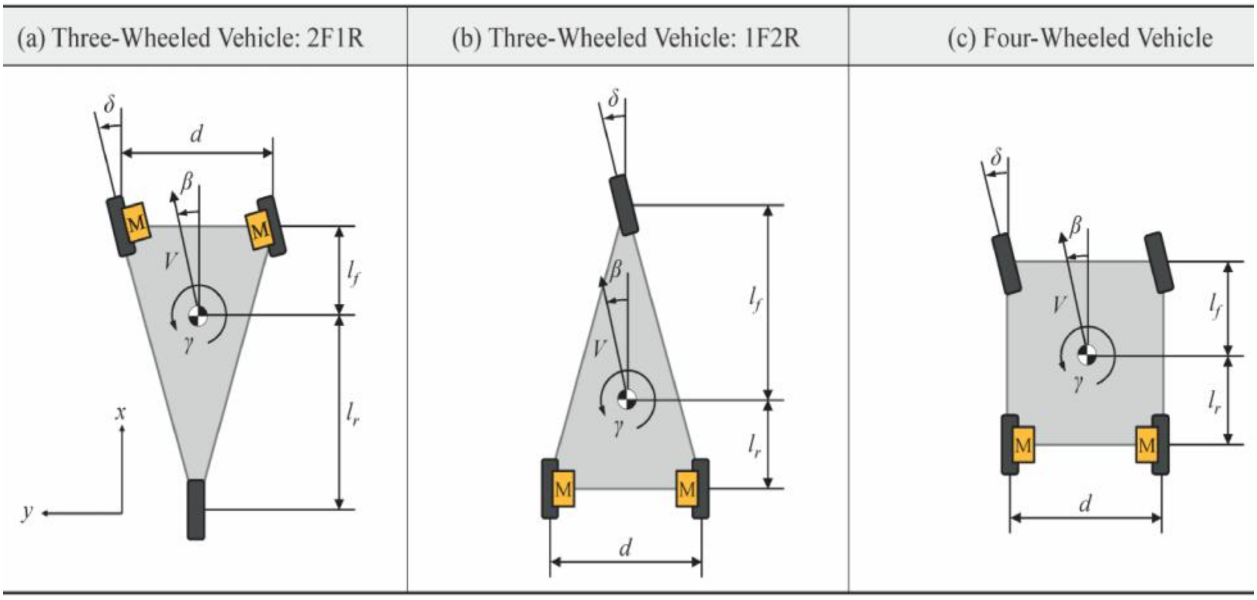

system on the vehicle dynamics is ignored; and the center of gravity of each system is assumed to be located at its geometric center of the base, i.e., each wheel negotiates with equally divided vertical load.

For all systems introduced in the analyses of this section, the state space representation is as expressed below:

$$\dot{x} = Ax + Bu \qquad ...(1)$$

$$y = Cx + Du \qquad ...(2)$$

where,

$$x = [\quad ¥]^T \qquad ...(3)$$

$$u = [¢ \ M_z]^T \qquad ...(4)$$

$$C = I \qquad ...(5)$$

$$D = 0 \qquad ...(6)$$

for all cases.

Three-Wheeled Vehicle and its Dynamics

Huston, Graves and Johnson first studied three-wheeled vehicle dynamics in 1982 (Huston *et al.*, 1982). They made stability comparisons between a three-wheeled vehicle with two wheels on the front axle (2F1R), a three-wheeled vehicle with two wheels on the rear axle (1F2R) and a standard four-wheeled vehicle, and concluded that three-wheeled vehicles can offer safe alternatives to four-wheeled vehicles.

Here, two dynamic models which Huston *et al.* (1982) proposed are introduced with some modifications: it is assumed that two independent driving motors are equipped, and the steering wheels are in the front in both cases.

Three-Wheeled Vehicle (2F1R) and its Dynamics

The schematic of the system is shown in Figure 1a. Two independent driving motors are attached in the front steering wheels, and a non-driving-nor-steering wheel is in the rear.

The governing equations are as below:

$$A = \begin{bmatrix} -\dfrac{2C_f + C_r}{mV} & -\dfrac{2l_f C_f - l_r C_r}{mV^2} \\ -\dfrac{2l_f C_f - l_r C_r}{I_z} & -\dfrac{2l_f^2 C_f + l_r^2 C_r}{I_z V} \end{bmatrix} \qquad ...(7)$$

$$B = \begin{bmatrix} \dfrac{2C_f}{mV} & 0 \\ \dfrac{2l_f C_f}{I_z} & \dfrac{1}{I_z} \end{bmatrix} \qquad ...(8)$$

Three-Wheeled Vehicle (1F2R) and its Dynamics

The schematic of the system is shown in Figure 1b. Two independent driving motors are attached in the rear wheels, and a non-driving steering wheel is in the front.

The governing equations are as below:

$$A = \begin{bmatrix} -\dfrac{C_f + 2C_r}{mV} & -\dfrac{l_f C_f - 2l_r C_r}{mV^2} \\ -\dfrac{l_f C_f - 2l_r C_r}{I_z} & -\dfrac{l_f^2 C_f + 2l_r^2 C_r}{I_z V} \end{bmatrix} \qquad ...(9)$$

$$B = \begin{bmatrix} \dfrac{C_f}{mV} & 0 \\ \dfrac{l_f C_f}{I_z} & \dfrac{1}{I_z} \end{bmatrix} \qquad ...(10)$$

Four-Wheeled Vehicle and its Dynamics

Although the dynamic analyses for four-wheeled ground vehicles are plentiful, most of them are concerning the conventional engine-

Figure 2: Distance to the Uncontrollability

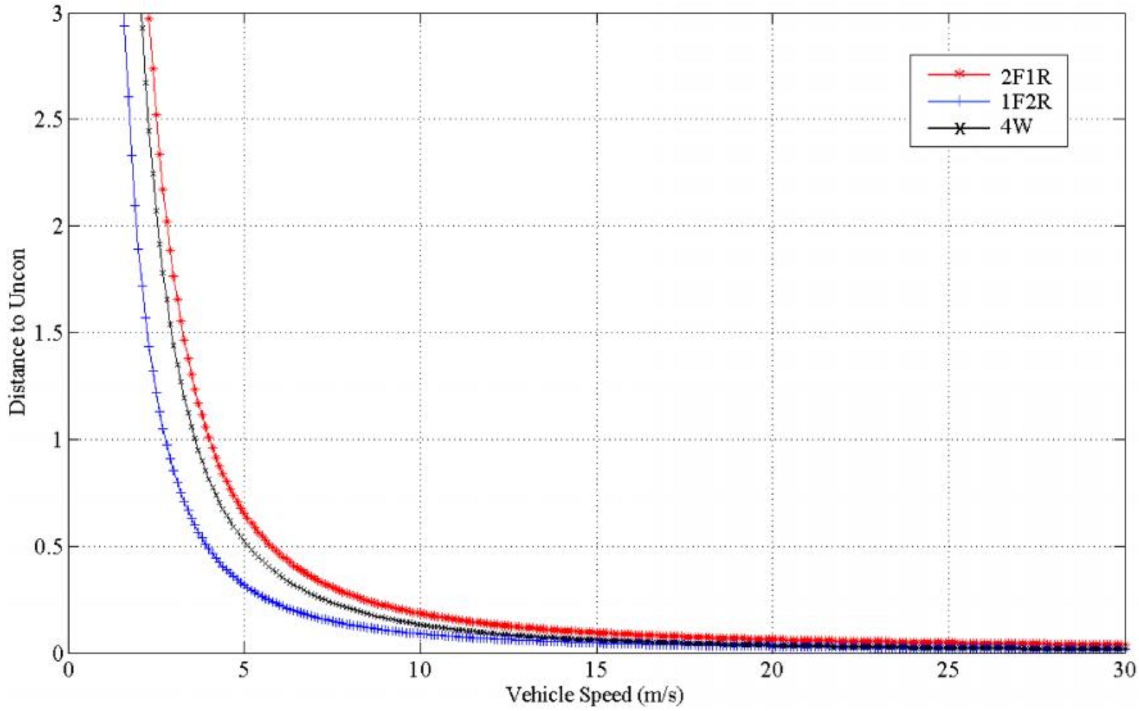

driven vehicles. Here, a dynamic model for an independent motor driven electric vehicle is introduced. The model is based on the bicycle model. The schematic of the system is shown in Figure 1c, and the governing equations are as below:

Structural Stability Evaluation

As the first step, vehicle's structural stability, which refers to the tip-over stability in this case, is evaluated. Previous research works have introduced numerous criteria to quantify the vehicle tip-over stability (Peters *et al.*, 2006), such as Static Stability Factor (SSF) (Hac, 2002), Load Transfer Metric (LTM) (Odenthal *et al.*, 1999), Energy Stability Margin (ESM) (Messuri *et al.*, 1985), and Force-Angle Stability Metric (FAS) (Papadopoulos *et al.*, 1996). By applying each of these criteria to the models introduced above, the structural stability is examined.

Evaluation results are shown in Table 1. Numbers are unitless, and the larger number indicates the better stability. Generally, 4-wheeled vehicle is the most structurally stable by all criteria, which can be explained by the fact that 4-wheeled vehicle has the largest base of support which is directly related to the tip-over moment.

Compatibility with EV

In order to see the compatibility of the system with EV motion control, the controllability and the system response of the vehicle dynamic models are evaluated. Firstly, the controllability of each system is checked. Secondly, yaw rate responses are shown with respect to the steering input and the yaw moment input respectively, since we are dealing with two major inputs which distinguish EVs from conventional engine vehicles from the motion control point of view.

Table 1: Structural Stability Summary			
Criterion	2F1R	1F2R	4W
SSF	0.74	0.74	1.11
LTM	7.26	7.26	10.89
ESM	16.78	16.78	18.63
FAS	poor when accel.	poor when braking	-

Table 2: Controllability Check			
	2F1R	1F2R	4W
rank($\Gamma_c[A,B]$)/Dimension	2/2	2/2	2/2
Controllability	YES	YES	YES

CONTROLLABILITY STUDY

First of all, using the state Equations (1)-(10), controllability of each system is checked. Controllability of a system can be clarified by calculating the rank of the matrix $\Gamma_c[A, B]$. The system is controllable if and only if $\Gamma_c[A, B]$ has full rank. This criterion is binary, i.e., it only provides 'YES-NO' answers, and the answers for the given systems are shown in Table 2.

For more in-depth comparison of the controllability of the different systems, a quantitative measurement is needed. In order to meet this demand, the method used is the quantification method introduced by Eising (Eising, 1984), which provides a standard to measure how far a controllable system is from an uncontrollable one. The distance «(A, B) between a controllable system from an uncontrollable one is defined as follows:

$$\text{«}(A, B) \equiv \min \pm_n (sI - A, B) \quad \text{...(13)}$$

where ±($sI - A$, B) is the smallest singular value of [sI – A, B]. This criterion indicates the spatial distance from a system to its nearest uncontrollable point, which means when «(A, B) = 0, the system becomes uncontrollable if there is any parameter deviation in the system. According to the definition, the distances for the given systems are shown in Figure 2.

All vehicle models are controllable. However, as seen in Figure 2, in terms of robustness the 3-wheeled vehicle with two wheels on the front is the most farthest from the uncontrollability, even farther than the 4-wheeled one. The result shows that the relative controllability of the 3-wheeled vehicle which has two wheels on the front, is higher than that of the 4-wheeled vehicle at any vehicle speed, which implies that the 2F1R vehicles are more robust against parameter variation than the 4-wheeled ones. This can be generalized, because the only parameter that varies in the matrices A and B and affects the result is the vehicle speed V, given that the system inputs remain the same.

Vehicle Yaw Response Analyses

For vehicle yaw response analyses, state equations are converted into transfer functions $G(s)$ as:

$$G(s) = C(sI - A)^{-1}B + D \quad \text{...(14)}$$

where, system inputs are defined in (4), and common output is the vehicle yaw rate ¥, which makes six transfer functions in total for the analyses. The details are omitted, and the results are shown in Figures 3-6.

Figure 3 shows the responses of the vehicle models in time domain when given a step steering input whose magnitude is 30 degrees which is usually the maximum value for passenger vehicles at $t = 0$. It can be seen that the 3-wheeled vehicle models are slower in response than the 4-wheeled one, however, the difference is not so significant; the vehicle speed is dominant, not the chassis structure. It can be confirmed in Figure 4. Thus it can be generally stated that vehicle's yaw response

Figure 3: Step Steering Input (30 degrees) vs. Vehicle Yaw Response

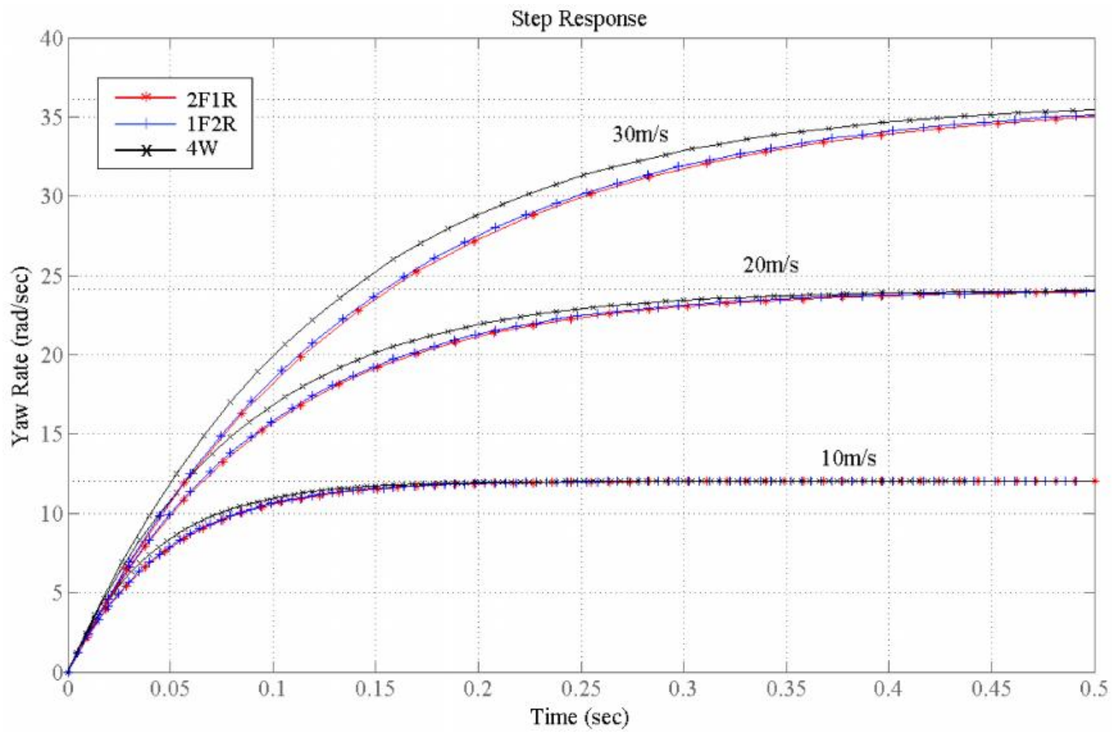

Figure 4: Bode Plot: Steering Input vs. Vehicle Yaw Response

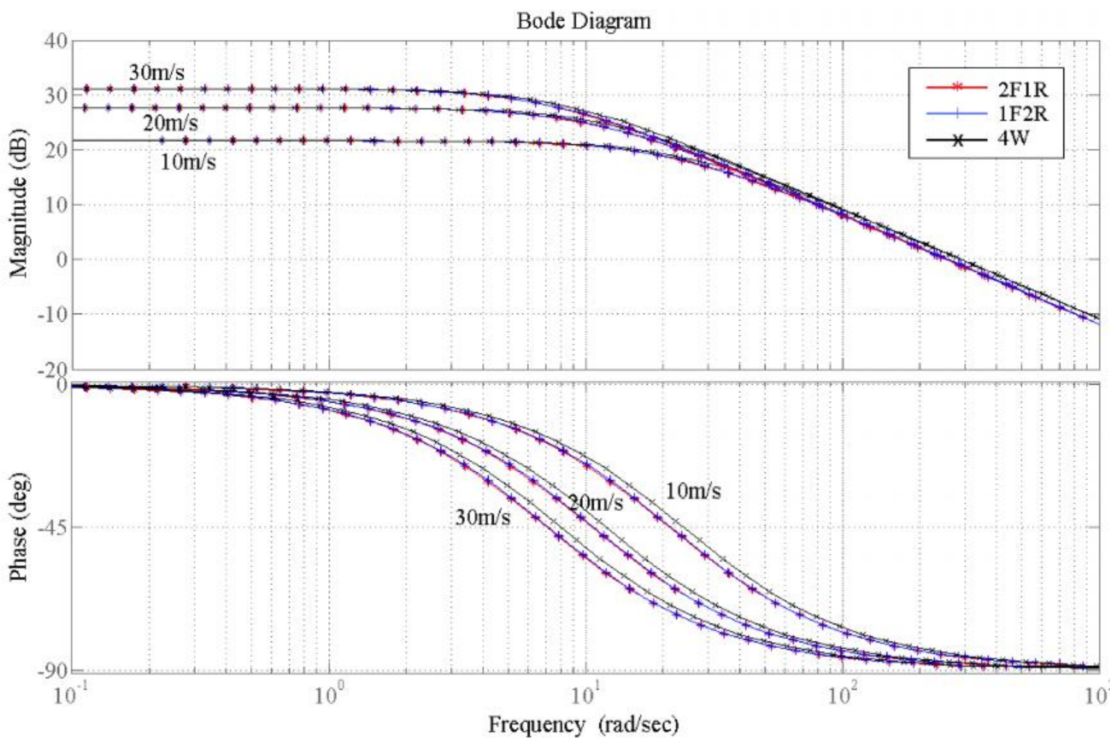

Figure 5: Step Direct Yaw Moment Input vs. Vehicle Yaw Response

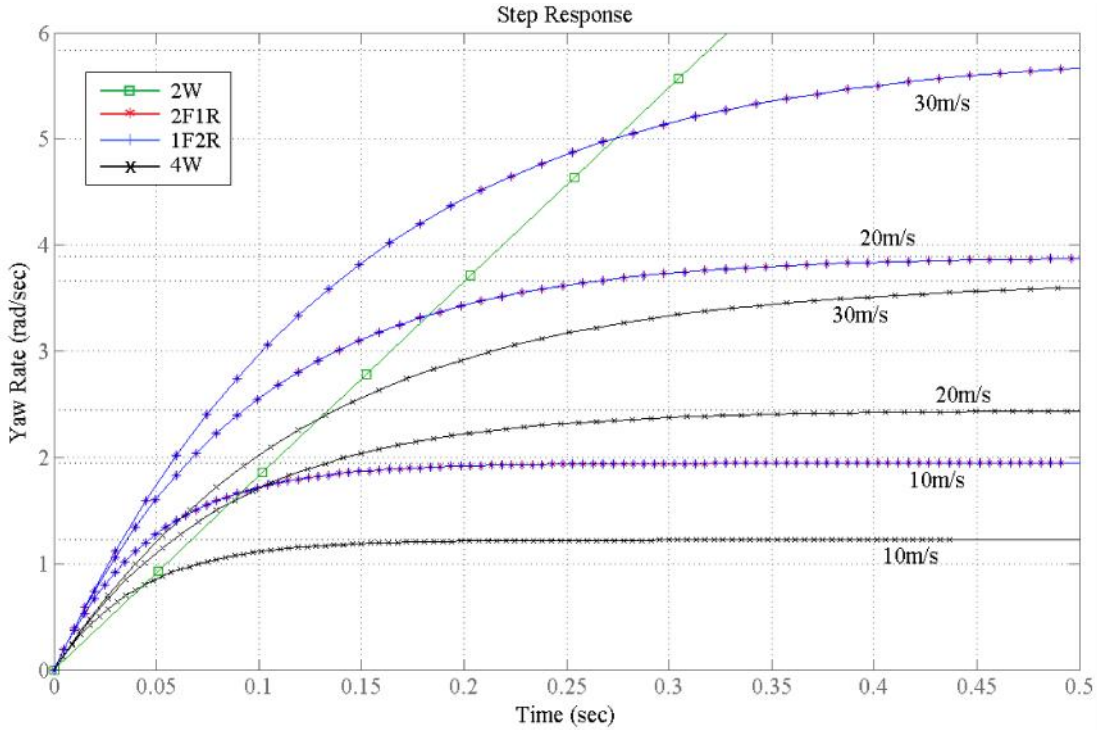

Figure 6: Bode Plot: Direct Yaw Moment Input vs. Vehicle Yaw Response

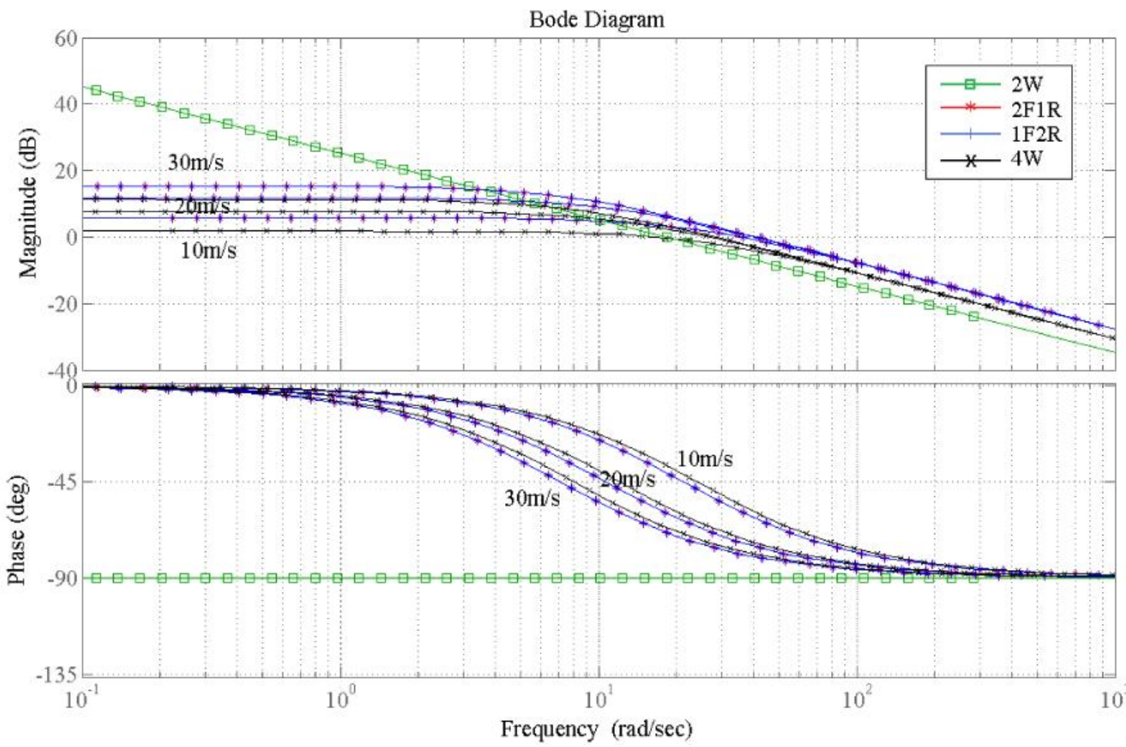

to the steering input is dependent on the vehicle speed.

When there exists the difference between traction forces generated by two driving wheels, yaw moment occurs in the vehicle, which distinguishes EVs from the conventional engine vehicles. This difference is regarded as another input variable: the direct yaw moment input.

Figure 5 shows the yaw responses of the vehicles in time domain when given a step direct yaw moment input whose magnitude is 80% of the vertical load of each case, which is usually the maximum friction on a dry asphalt, at $t = 0$. It can be seen that the response speed of the 3-wheeled vehicles is faster than that of the 4-wheeled one. Moreover, the steady state gain of the 3-wheeled vehicles is remarkably larger than that of the 4-wheeled one at any longitudinal speed. This difference in gain can be explained by examining the transfer functions governing the dynamics.

$$G(0)\text{¥}\, M_z = \begin{cases} \dfrac{V(2C_f + C_r)}{2L^2 C_f C_r \left(1 - \dfrac{m(2l_f C_f - l_r C_r)V^2}{2C_f C_r L^2}\right)} = \dfrac{3V}{8L^2 C_0} \\ \dfrac{V(C_f + 2C_r)}{2L^2 C_f C_r \left(1 - \dfrac{m(l_f C_f - 2l_r C_r)V^2}{2C_f C_r L^2}\right)} = \dfrac{3V}{8L^2 C_0} \\ \dfrac{V(2C_f + 2C_r)}{4L^2 C_f C_r \left(1 - \dfrac{m(l_f C_f - l_r C_r)V^2}{2C_f C_r L^2}\right)} = \dfrac{V}{3L^2 C_0} \end{cases} \quad \ldots(15)$$

where C_0 is an arbitrary coefficient. From this observation, it is obvious that the difference in gain results from the difference of cornering stiffness, which is a mechanical stiffness hindering the direct yaw moment input from turning the vehicle.

Moreover, in Figure 6 it can be seen that the frequency response is almost the same as Figure 4, but there only exists difference in gain. Such relatively small gain makes it difficult for the direct yaw moment input to contribute to EV motion control. Improvements need to be made here to fully utilize two inputs of the independent motor driven EVs.

To summarize, the three-wheeled vehicles are less structurally stable than the four-wheeled one. They have, however, larger gains in yaw rate response to the yaw moment step input, which is a desirable property in motion control using independent driving motors. Especially the three-wheeled model with two front wheels has almost the same response to the unit step steering input, compared to the four-wheeled model, whereas it shows better response to the yaw moment input. Thus, considering the vehicle motion control using independent driving motors, the three-wheeled vehicle can be an attractive alternative.

From the observations made here, it is clear that when trying to find a novel chassis structure for the independent motor driven EVs, there are some efforts to be made: to reduce mechanical stiffness hindering the direct yaw moment input from turning the vehicle, and to maintain structural stability and controllability of the system, which forms the background of the proposed system design.

EXPERIMENTAL VEHICLE AND MODELING

Based on the observations and consequent conclusions made in the previous section, this work proposes a novel structure using caster wheels and independent driving motors, as one of the possible chassis configurations for the future personal mobility solution. The system consists of two independent driving wheels and two caster wheels. This configuration enables the vehicle to have: a low mechanical stiffness against the direct yaw moment input because caster wheels can rotate freely, and a high static stability because the vehicle has four wheels, which showed the highest static stability from the observation in the previous section.

In order to demonstrate the feasibility of the proposed system, an experimental vehicle which has two driving wheels and two caster wheels was fabricated. Before fixing the actual configuration, contemplation was needed to decide where to put the caster wheels: front or rear. Vehicles which require high agility such as forklift, whose operational space is restricted, often have steering wheels in the rear, because steering wheels on the rear axle enable high yaw rates to make sharp turns. However, nearly all passenger vehicles have steering wheels on the front for better stability. An obvious difference between these two types of vehicle is the operational speed range.

Figure 3 shows the change in distance from uncontrollability, when damping and stiffness about the king pin of the casters change. It is shown that configuration with casters on the front has better controllability over the counterpart. Note that the system with casters in the rear always falls uncontrollable at a certain damping level. Based on the results of the simulation above, the experimental vehicle

Figure 7: Distance from Uncontrollability (Vertical Axis, Unitless), While Changing Damping Coefficient D (Horizontal Axis, Nm/(rad/s) and Stiffness K (Depth, Nm/rad). (a) Casters in the Front at V = 1 m/s; (b) Casters in the Front at V = 10 m/s; (c) Casters in the Front at V = 20 m/s; (d) Casters in the Rear at V = 1 m/s; (e) Casters in the Rear at V = 10 m/s; and (f) Casters in the Rear at V = 20 m/s

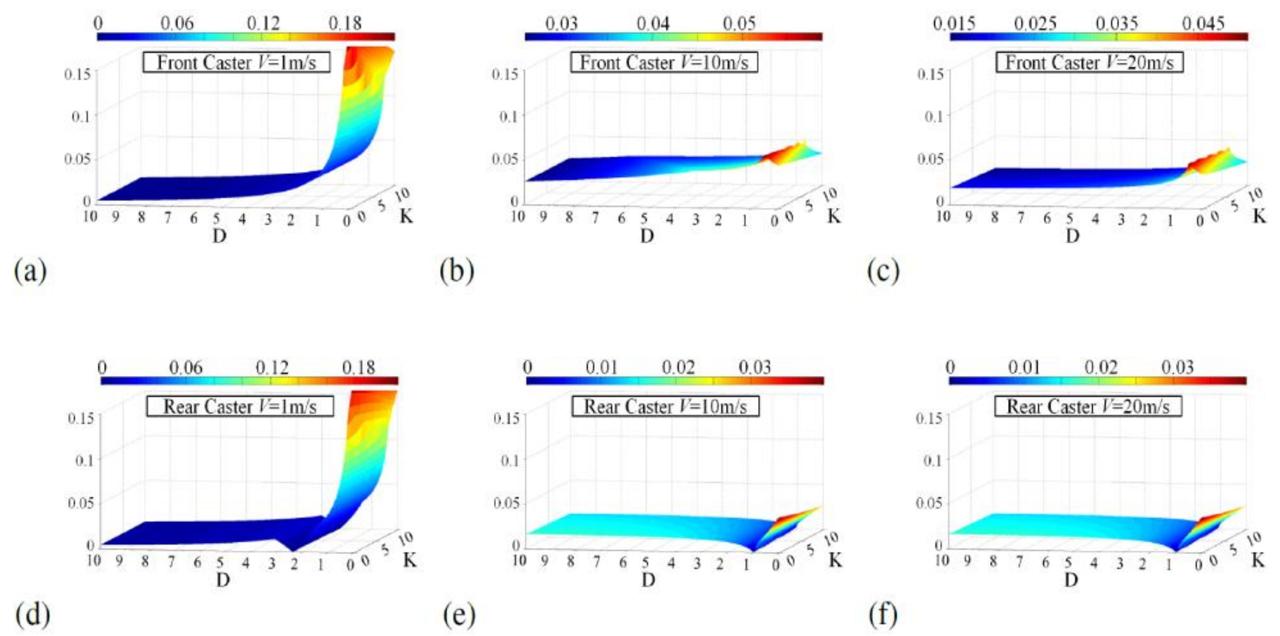

Figure 8: Caster Wheeled Electric Vehicle CIMEV: Two Rear Wheels are Driven via Belt and Pulley by Two Independent Driving Motors (90 Watts Each). Two Front Wheels are Casters, Connected via Gears to Two Independent Steering Motors (60 Watts Each)

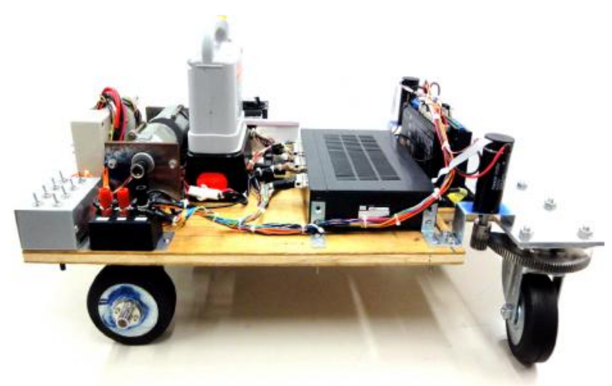

is designed. Driving motors are equipped in the rear, and casters in the front.

Experimental Vehicle, CIMEV

Caster-wheeled Independent Motor-driven Electric Vehicle (CIMEV) is designed to run unmanned. It is controlled by a digital signal processor (S-BOX) with two input signals transmitted through a radio controller. The PWM signals interpreted by the receiver are sent into the DSP, where they are linearized to drive the motors—both driving and steering—to run the vehicle. Four independently controlled electric motors are used. Two are used for steering and the other two for driving. The vehicle is powered by a 24 V Ni-MH battery. System configuration is shown in Figure 9. More details of the experimental vehicle are shown in (Kim *et al.*, 2011).

Modeling

The dynamic model suggested by Somieski (Somieski, 1997) seems to be compatible for the system. The system is modeled neglecting the existence of steering motors, and it is

Figure 9: System Configuration of the Experimental Vehicle CIMEV: The Vehicle is Controlled by a Digital Signal Processor (S-BOX) with a Remote Controller. Its Dynamic Behavior is Monitored and Recorded Through an Acceleration Sensor Unit and Four Encoders

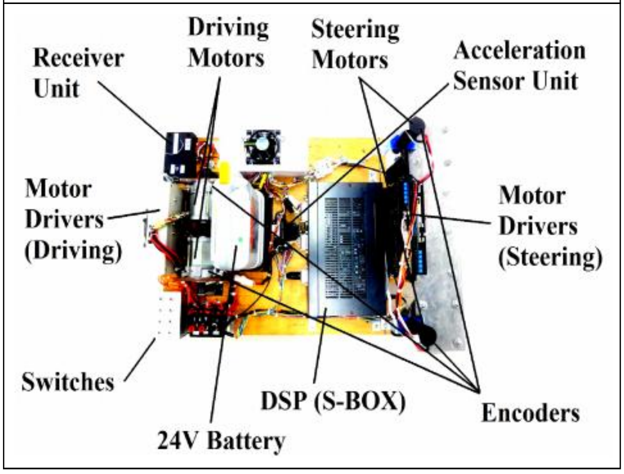

assumed that the casters are free to rotate only under the effect of the stiffness *K* and the damping *D* about the king pin. The governing equations are written as:

$$I_w \ddot{\text{¢}} + D\dot{\text{¢}} + K\text{¢} = -M_{sa}(\sim) - eF_y(\sim) - D_t(V)\dot{\text{¢}} \quad ...(16)$$

$$\sim\, = \text{¢} - {}^{-}v \quad ...(17)$$

Considering the size and the type of the wheel we are dealing with, which is 0.1 m in diameter and made of hard-rubber, the terms $M_{sa}(\sim)$ and $D_t(V)\dot{\text{¢}}$ can be neglected. Moreover, since $F_y(\sim)$ can be approximated into a linear form of $F_y(\sim) = C_f\sim$, we can simplify (16) to (18) below, where the theoretical backgrounds can be found in (Bakker *et al.*, 1987; Pacejka, 1992; Abe, 2008; and De Falco *et al.*, 2010):

$$I_w \ddot{\text{¢}} + D\dot{\text{¢}} + K\text{¢} = -eC_f\sim \quad ...(18)$$

As the experimental vehicle has been provided with two steering motors, equations can be written as below, considering the torque inputs of the steering motors, and regarding that the liaison moments and the equivalent forces are given by the motors:

$$I_w \ddot{\text{¢}}_L + eC_f \text{¢}_L = eC_f \quad + \frac{el_f C_f}{V} \text{¥} + T_{mL} \qquad ...(19)$$

$$I_w \ddot{\text{¢}}_R + eC_f \text{¢}_R = eC_f \quad + \frac{el_f C_f}{V} \text{¥} + T_{mR} \qquad ...(20)$$

$$I_z \text{¥} = \frac{l_f}{e}(T_{mL} + T_{mR}) - 2l_r C_r \left(\quad - \frac{l_r}{V} \text{¥} \right) + M_z \qquad ...(21)$$

$$mV\left(\dot{} + \text{¥} \right) = \frac{1}{e}(T_{mL} + T_{mR}) + 2C_r \left(\quad - \frac{l_r}{V} \text{¥} \right) \qquad ...(22)$$

Control Strategies and Advantages of the Proposed System

The global control scheme for CIMEV is shown in Figure 10. The upper-level controller computes the direct yaw moment reference and the lateral force reference in the form of the steering angles in order to meet the speed and yaw rate requirements. The lower-level controllers which are the driving controller and the steering controller, assign the motor torques to give the vehicle speed, yaw rate, and the steering angles.

Experiments were done to show the advantages of the proposed system: high mobility, lateral force observer, load transfer estimation, under-steer gradient control, and bank angle estimation. The experiment results are shown, and the corresponding advantages of the system are discussed.

High Mobility

Figure 11 shows the experimental result of the vehicle yaw rate responses to the direct yaw moment input versus the conventional steering maneuver at 90 degrees cornering at a low speed of 1 m/s. For the conventional steering case, the steering angle was given by Ackermann geometry at 30 degrees which is usually the maximum for passenger vehicles.

Figure 10: Block Diagram of the Global Control Scheme for CIMEV

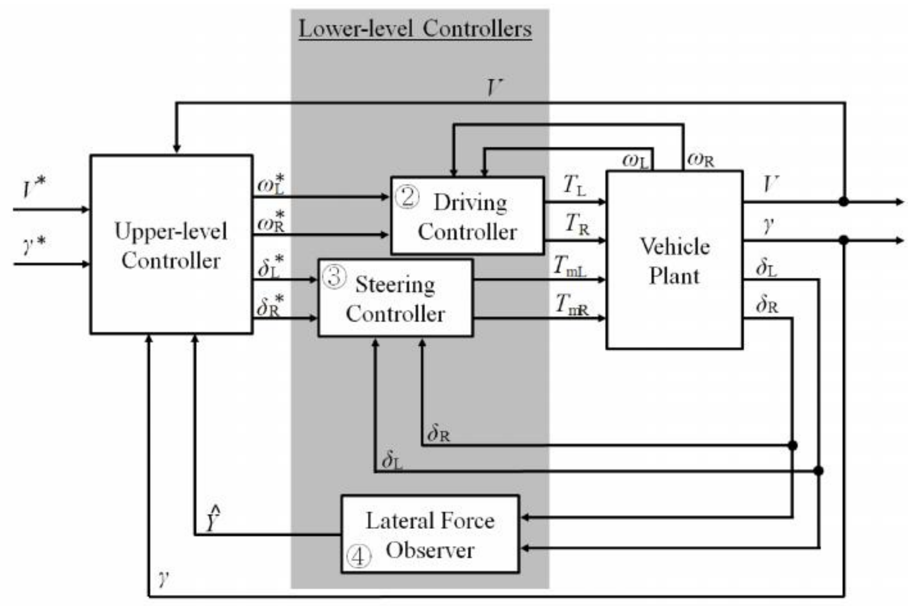

Figure 11: Yaw Rate Responses to the Direct Yaw Moment Input versus the Conventional Steering Maneuver at 90 degrees Cornering. Vehicle Speed is 1 m/s in all Cases. The Steering Angle is 30 degrees at Inner Wheel for the Conventional Steering Case. Direct Yaw Moment is Given by Wheel Speed Controller

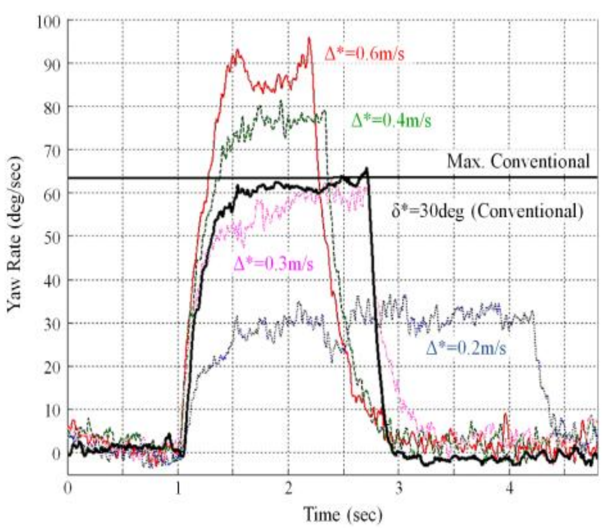

It is shown that the yaw rate can go over the maximum rate of the conventional one at a given speed, by applying direct yaw moment to the driving wheels without causing any energy loss from cornering resistance, which is consistent with the observation results from the system analyses. This property enables CIMEV to make a sharper turn than a conventionally steered vehicle, so that CIMEV can move more freely in restricted spaces. This experiment result also can be associated with the ICR location shown in Figure 12. Usually a normal passenger vehicle has the minimum turning radius of 5 meters, meanwhile CIMEV can turn with zero radius.

At low speed, the advantage of using caster wheels is obvious: as the way they are defined, they freely rotate and so does the vehicle. Vehicles with the normal steering system, need to run in order to make turns. CIMEV, on the other hand, can make turns at speed of zero. This property is advantageous not only for the passenger EV applications, but also for the vehicles or the mobile robots which work in restricted spaces.

Figure 12: Possible Location of ICR (Instant Center of Rotation), Colored Blue. CIMEV (Upper) and Conventional One (Lower). Vehicle with Normal Steering has Usually 5 meters of Minimum Turning Radius, While CIMEV has Zero at Zero Vehicle Speed

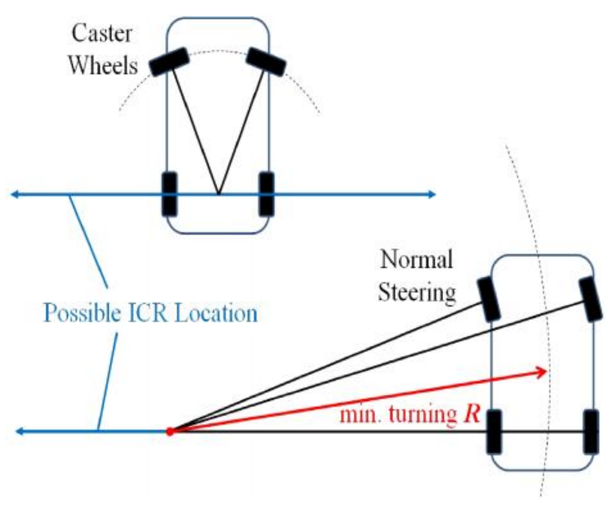

Making Use of Lateral Force Observer

Since CIMEV is equipped with two independent steering motors, it is possible to apply disturbance observers in the control logic of each wheel. From Equations (19) and (20), if we define the disturbance torques for the left and right as:

$$T_{dL} = eC_f \quad + \frac{el_f C_f}{V} ¥ - eC_f ¢_L = eC_f \sim_L \simeq eY_L \qquad ...(23)$$

$$T_{dR} = eC_f \quad + \frac{el_f C_f}{V} ¥ - eC_f ¢_R = eC_f \sim_R \simeq eY_R \qquad ...(24)$$

the lateral force can be simply calculated by dividing the caster length e without using any special sensors to measure it. Moreover, by controlling the steering angles, the vehicle is allowed to have the controlled lateral forces, which gives a number of implications to vehicle motion control field.

Figure 13 compares the lateral forces between the one calculated using disturbance observers and the one using acceleration sensor. Since it is a steady state circle running condition (i.e., ¥ = 0 and $M_z = 0$), disturbance torques were converted into lateral forces (red and blue dashed lines), and the lateral acceleration was converted into the necessary net lateral force to make the turn (black solid line). Experimental result shows that the lateral force estimation using disturbance observer has reliable accuracy when compared with the calculation using acceleration sensor.

Figure 13: Lateral Forces Calculated by Using Disturbance Observer versus the One Calculated by Using Lateral Acceleration Sensor During a Steady State Circle Running. Vehicle Speed was 2 m/s, and the Steering Angle was 15 degrees at Inner Wheel

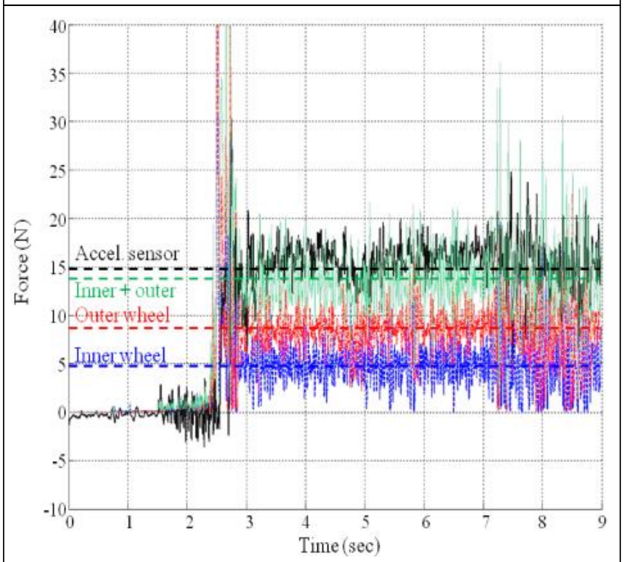

The results are comparable to Yih's work (Yih *et al.*, 2004) that proposed a novel sideslip estimation method using steering torque information and a disturbance observer. The work provides many practical implications, however, there still remain a number of model uncertainties, or approximated parameters in calculation, which eventually dull down the estimation accuracy, whereas CIMEV consists of a simpler mechanical configuration which imposes less model uncertainties on the estimator—the disturbance observer.

DISCUSSION ON LOAD TRANSFER

As seen in Figure 13, the estimated lateral force has larger value for the outer wheel than the inner one. In this work, it is assumed that the cornering stiffness C_f has a fixed value, however, in reality the value changes due to the dynamic change in vertical load. It is found, from the experimental result and from the definition of C_f in (Abe, 2008), that the ratio of the vertical load is around 0.63 between the inner and outer wheels.

On the other hand, from the experiment condition, and the vehicle geometry and parameters, for a given lateral acceleration, the vertical load of the front wheels can be roughly calculated as:

$$N_{zFL} = \frac{mgl_r}{L} + \frac{2mhl_r}{dL} a_y \quad ...(25)$$

$$N_{zFR} = \frac{mgl_r}{L} - \frac{2mhl_r}{dL} a_y \quad ...(26)$$

where, a_y of this experiment was 1.87 m/s^2, thus the ratio N_{zFL}/N_{zFR} should be around 0.69, which is fairly close to the value from the experiment result. This observation implies that, by using the lateral force observer, the dynamic load transfer of a running vehicle can be calculated without attaching any special sensors such as a potentiometer. More investigation needs to be done for better accuracy.

Under-Steer Gradient Control

Furthermore, it is also possible at a high vehicle speed to change the under-steer characteristics by using the lateral force feedback control. In this paper, this will be referred as the under-steer gradient control. The under-steer gradient K_{us} is one of the major vehicle dynamic characteristics during cornering.

CIMEV inherently is a severely under steered vehicle due to the free rotation of the casters, however, by using this control it becomes close to a neutral steered one. The under-steer gradient controller makes $\sim_f$ smaller by giving the positive feedback of the estimated lateral force $\hat{Y}$ to the direct yaw moment M_z, and thus it virtually makes the cornering stiffness C_f larger: refer to (Abe, 2008). Consequently K_{us} can be controlled to approach zero. The control scheme is shown in Figure 14, and the experimental results are shown in Figures 15 and 16. The vehicle ran on a circle and was accelerated from 0 to 4 m/s.

Usually a passenger vehicle is under-steered, and has a peak in yaw rate gain at a certain vehicle speed called the characteristic speed V_{char}, like the red dotted case in Figures 15 and 16, so the radius of cornering gets bigger as the vehicle accelerates. On the other hand, the neutral steered vehicle can run on a circle of a constant radius regardless of its speed, which gives the driver a natural (linear) feeling during cornering. Using the under-steer gradient control, the cornering characteristics of CIMEV can be tuned to the driver's favor, i.e., the value can be controlled by changing the gain Clat as shown in Figure 15.

Bank Angle Estimation

Another advantage of using the lateral force observer is the estimation of the road bank angle on which the vehicle is running. It is based on a simple kinematic relation between the gravitational force and the lateral force of the front wheels as shown in Figure 17 without using any special sensors. When a vehicle is running straight on a road which has a bank angle of ¨, from the kinematic relation it is expressed as:

Figure 14: Under-Steer Gradient Controller

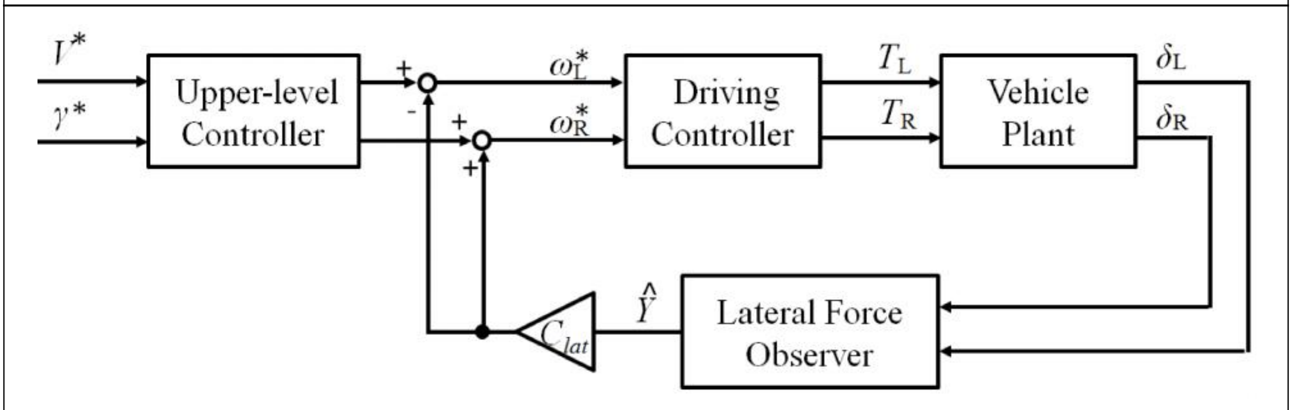

Figure 15: Under-Steer Gradient Control: Change in Slope (Under-Steer Gradient K_{us})

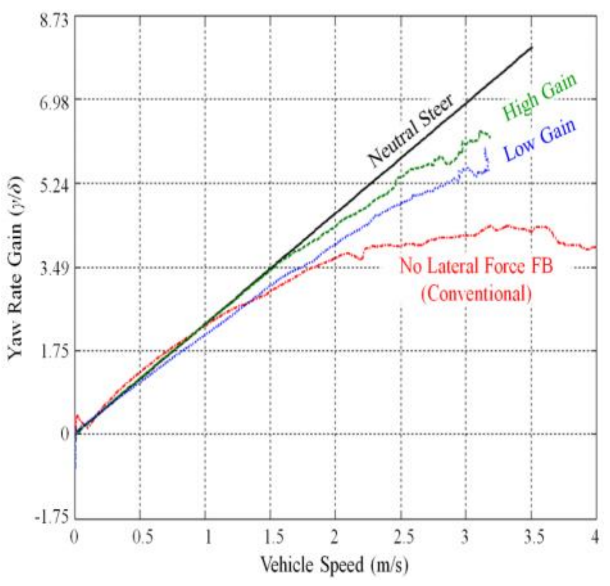

Figure 16: Under-Steer Gradient Control: Vehicle Trajectory During an Accelerating Circle Run

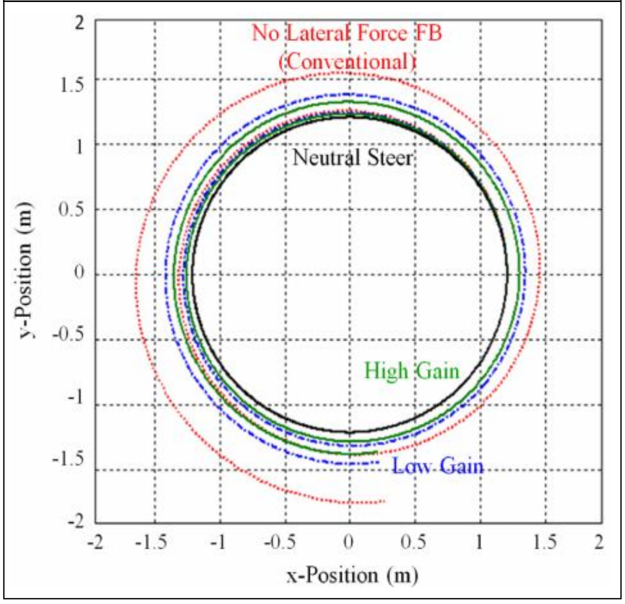

Figure 17: Kinematic Relations of Bank Angle Estimation

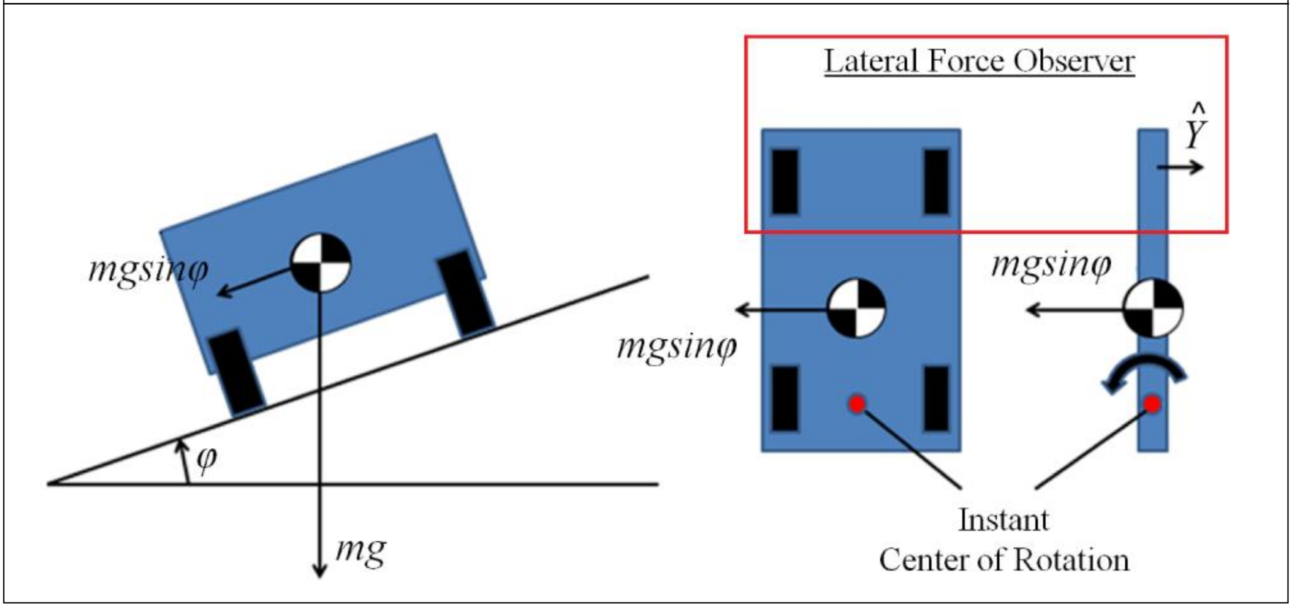

$$\hat{Y} = \frac{l_r}{L} mg \sin\varphi \qquad ...(27)$$

thus φ can be estimated as:

$$\hat{\varphi} = \sin^{-1}\frac{\hat{Y}L}{l_r mg} \simeq \frac{\hat{Y}L}{l_r mg} \qquad ...(28)$$

It can be seen in Figure 19 that the two lateral acceleration signals agree well, and the estimated and measured values are acceptable. The bank angle of the road is 10.5 degrees, which assigns 1.79 m/s^2 of lateral acceleration due to gravity. The vehicle was

Figure 18: Bank Where the Experiment was Carried Out. The Bank Angle is 10.5 degrees

Figure 19: Lateral Acceleration Signal from the Acceleration Sensor and the Lateral Force Observer. Vehicle is Released at $t = 2$, and the Vehicle Speed Increases Up to 2 m/s

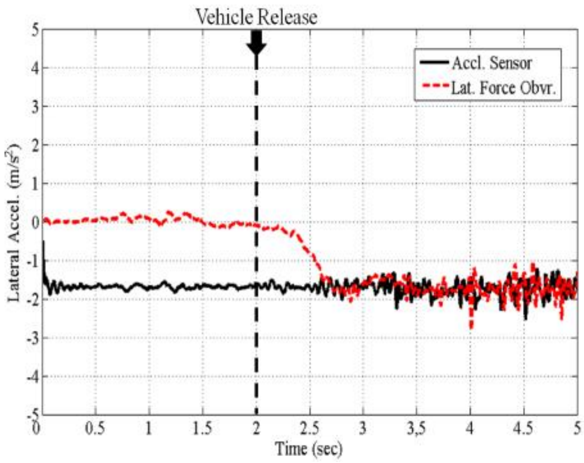

released at *t* = 2 by hand, and the vehicle speed increases up to 2 m/s. As the vehicle starts to run, the lateral force observer works properly.

It is a simple and cost effective method, however in order to apply this method to a passenger vehicle, decoupling the effects of the bank angle and the lateral acceleration during cornering needs to be investigated. Ryu *et al.* (2004) have worked on this issue, using the Global Positioning System (GPS) and the Internal Navigation System (INS) (Ryu *et al.*, 2004). GPS and INS nowadays are good enough for vehicle state estimation, however, the use of external information, especially GPS, can be a potential risk factor. The proposed mechanism of this work is applicable to eliminate the risk of using external information, by providing the exact measurement internally using kinematics.

CONCLUSION

In this paper, a novel chassis structure for electric vehicles is proposed using caster wheels and independent driving motors, after a thorough study on wheel placements and compatibility with EVs. An actual experimental vehicle is introduced, and its system configuration is shown. Feasibility and the advantages of the system is shown with experiment results. At low speed, CIMEV shows high mobility. It is applicable in various fields such as passenger EVs, mobile robots, military and space rovers which work in limited spaces. Additionally, utilizing lateral force observer, the lateral force during cornering can be estimated and possibly controlled. By doing so it is possible to reduce energy loss from the cornering resistance, or to control the characteristics of the vehicle such as the under-steer gradient.

REFERENCES

1. Abe M (2008), *Automotive Vehicle Dynamics*, p. 69, Theory and Applications, TDU Press.
2. Ando N and Fujimoto H (2009), "Fundamental Study of Yaw-Rate Control for Four Wheel Independent Drive Electric

Vehicle with Driving/Braking Force Distribution of In-Wheel Motors", *IEEJ Technical Meeting Record*, pp. 13-18.

3. Bakker E, Nyborg L and Pacejka H B (1987), "Tyre Modeling for Use in Vehicle Dynamics Studies", SAE Paper No. 870421.

4. Borenstein J and Koren Y (1985), "A Mobile Platform for Nursing Robots", *IEEE Transactions on Industrial Electronics*, Vol. 32, No. 2, pp. 158-165.

5. Brienza D M and Brubaker C E (1999), "A Steering Linkage for Short Wheelbase Vehicles: Design and Evaluation in a Wheelchair Power Base—A Technical Note", *Journal of Rehabilitation Research and Development*, Vol. 36, No. 1, pp. 42-47.

6. De Falco D, Di Massa G and Pagano S (2010), "On the Castor Dynamic Behavior", *Journal of the Franklin Institute*, Vol. 347, pp. 116-129.

7. Ebihara T, Moriguchi K and Hayashi K (2011), "Electric Ride-on Mower", International Patent Application No. WO2011/092908.

8. Eising R (1984), "The Distance Between a System and the Set of Uncontrollable Systems", *Lecture Notes in Control and Information Sciences*, Vol. 58, pp. 303-314.

9. Hac A (2002), "Rollover Stability Index Including Effects of Suspension Design", SAE Transaction No. 2002-01-0965.

10. Hori Y (2004), "Future Vehicle Driven by Electricity and Control—Research on Four-Wheel-Motored 'UOT Electric March II'", *IEEE Transactions on Industrial Electronics*, Vol. 51, No. 5, pp. 954-962.

11. Huston J C, Graves B J and Johnson D B (1982), "Three Wheel Vehicle Dynamics", *SAE Transaction*, Vol. 91.

12. Kim Y, Fujimoto H and Hori Y (2011), "Realization of Steer-by-Wire System for Electric Vehicles Using Caster Wheels and Independent Driving Motors", ICPE 2011 Proceedings.

13. Lam T L, Qian H and Xu Y (2010), "Omnidirectional Steering Interface and Control for a Foul-Wheel Independent Steering Vehicle", *IEEE Transactions on Mechatronics*, Vol. 15, No. 3, pp. 329-338.

14. Lee C and Lee T (1990), "Stability Analysis of Three and Four Wheel Vehicles", *JSME International Journal*, Vol. 33, No. 4.

15. Messuri D A and Klein C A (1985), "Automatic Body Regulation for Maintaining Stability of a Legged Vehicle During Rough-Terrain Locomotion", *IEEE Journal Robotics and Automation*, Vol. RA-1, pp. 132-141.

16. Mohan S K (2005), "Torque Vectoring Systems: Architecture, Stability Performance and Efficiency Considerations", Proceedings of the 6th All-Wheel Drive Congress.

17. Nam K, Fujimoto H and Hori Y (2012), "Lateral Stability Control of In-Wheel-Motor-Driven Electric Vehicles Based on Sideslip Angle Estimation Using Lateral Tire Force Sensors", *IEEE Transactions on Vehicular Technology*, Vol. 61, No. 5, pp. 1972-1985.

18. Odenthal D, Bünte T and Ackerman J (1999), "Nonlinear Steering and Braking Control for Vehicle Rollover Avoidance", European Control Conference Proceedings.

19. Pacejka H B (1992), "Modeling of the Pneumatic Tire and its Impact on Vehicle Dynamics Behavior", Lecture Series DR 6.04, Carl-Cranz-Gesellschaft e.V, Oberpfaffenhofen.

20. Papadopoulos E and Rey D (1996), "A New Measure of Tip Over Stability Margin for Mobile Base Manipulators", IEEE International Conference on Robotics and Automation Proceedings, pp. 3111-3116.

21. Peters S C and Iagnemma K (2006), "An Analysis of Rollover Stability Measurement for High-Speed Mobile Robots", IEEE International Conference on Robotics and Automation Proceedings.

22. Ryu J and Gerdes J C (2004), "Estimation of Vehicle Roll and Road Bank Angle", Proceedings of American Control Conference, Vol. 3.

23. Sawase K, Ushiroda Y and Miura T (2006), "Left-Right Torque Vectoring Technology as the Core of Super All Wheel Control (S-AWC)", *Mitsubishi Motors Technical Review*, No. 18, pp. 16-23.

24. Slay R A (1968), "Motor-Driven Wheeled Vehicles", United States Patent No. 3,404,746.

25. Somieski G (1997), "Shimmy Analysis of a Simple Aircraft Nose Landing Gear Model Using Different Mathematical Methods", *Journal of Aerospace Science and Technology*, No. 8, pp. 545-555.

26. Sumiya H and Fujimoto H (2012), "Electric Vehicle Range Extension Control System Based on Front- and Rear-Wheel Sideslip Angle and Left- and Right-Motor Torque Distribution", *IEEJ Transactions on Industry Applications*, Vol. 132, No. 3, pp. 308-314.

27. Swisher M B, Boothe L and Boothe G L (1952), "Powered Caster Wheel for Vehicles", United States Patent No. 2,582,177.

28. Yih P, Ryu J and Gerdes J C (2004), "Vehicle State Estimation Using Steering Torque", Proceedings of American Control Conference, Vol. 3.

APPENDIX

Nomenclature

a_y	lateral acceleration
C_f	cornering stiffness, front
C_r	cornering stiffness, rear
C_{lat}	understeer gradient control gain
d	tire track
D	caster's damping coefficient about king pin
D_t	damping moment due to tire tread width
e	caster arm length
F_y	lateral force at wheel-ground interface, general
h	distance from CG to road surface
I_w	caster's moment of inertia about king pin
I_z	vehicle's yaw moment of inertia about z-axis, CG
K	caster's elastic coefficient about king pin
K_{us}	vehicle's understeer gradient
L	vehicle's wheel base
l_f	distance from CG to front axle
l_r	distance from CG to rear axle
m	vehicle total mass
M_{sa}	self aligning torque
M_z	direct yaw moment input
N_{zFL}	vertical load at wheel, front-left
N_{zFR}	vertical load at wheel, front-right
T_L	driving motor torque, left
T_R	driving motor torque, right
T_{dL}	disturbance torque at steering motor, left
T_{dR}	disturbance torque at steering motor, right
T_{mL}	steering motor torque, left
T_{mR}	steering motor torque, right
V	vehicle speed
$\hat{Y}$	estimated total lateral force
Y_L	lateral force at wheel-ground interface, left
Y_R	lateral force at wheel-ground interface, right
α	wheel side slip angle
β	vehicle side slip angle
γ	vehicle yaw rate
δ	wheel steering angle
Δ	speed difference between inner and outer wheel
θ_V	direction of vehicle velocity at wheel
ϕ	road bank angle
$\hat{\phi}$	estimated road bank angle
ω_L	driving wheel speed, left
ω_R	driving wheel speed, right